

## Analysis of Internal Solitary Waves in SAR images based on theoretical model solutions for a two-layer stratified ocean

João Antonio Lorenzetti<sup>1</sup>  
Fabian Gualdas Dias<sup>2</sup>

<sup>1</sup> Instituto Nacional de Pesquisas Espaciais - INPE/DSR  
CEP 12227-010 – São José dos Campos - SP, Brazil  
loren@dsr.inpe.br

<sup>2</sup> Fundação do Meio Ambiente - FATMA  
Rua Padre Bernardo Freuser, 227 - Tubarão - SC, Brazil  
fabiandias@fatma.sc.gov.br

**Abstract.** Internal Solitary Waves (ISW) are waves that develop in the interior of a stratified ocean normally as a consequence of non-linear processes acting on tidal internal waves that interact with steep topography over the continental shelf or slope. They can be observed in SAR images due to the modulation produced on short-wave roughness on the sea surface caused by the ISW surface flow convergences/divergences. By analyzing the changes of the ISW packages from positive to negative  $\sigma_\theta$  SAR anomalies it is possible to infer some characteristics of these coherent features as well as of the water column such as the mean thermocline depth and vertical stratification. These inferences are made based upon theoretical solutions for a two-layer ISW model and a set of parameters extracted from the SAR images. The application was done for ISW waves observed in the SE Brazilian continental shelf.

**Keywords:** internal solitary waves, SAR, remote sensing, image processing, oceanography, ondas internas solitárias, sensoriamento remoto, processamento de imagens, oceanografia.

### 1. Introduction

Internal Solitary Waves (ISW), non-linear coherent features produced in the interior of the ocean by the internal baroclinic tides, are frequently observed in SAR images, particularly wherever tidal currents and vertical stratification occur near significant seafloor topographic features, such as shelf break zones, plateaus, or sills (Apel and Gonzalez 1983). A common case is where the ISWs are produced as oscillatory perturbations of the thermocline, the sharp discontinuity between the warm surface mixed layer and the colder deeper waters. They are visible in SAR images normally as packets of 2-8 bright and dark stripes which are separated by the wavelength of the internal tide (da Silva et al. 2007). When in deep water and the upper layer is shallower than lower layer, ISWs correspond to depression perturbations on the thermocline (i.e. thermocline deepens during the passage of the wave). This case corresponds to sequences of bright/dark anomalies of  $\sigma_\theta$  in a SAR image. When depth decreases to a point in which the upper layer is deeper than the bottom layer, ISWs change sign and become elevation perturbations on the thermocline and appear in SAR images as dark anomalies leading the bright ones. If in a single SAR image we can observe several ISW packets propagating towards the coast and consequently to shallower depths, and there is an inversion of polarization in their SAR signatures, then we can presume there is a region in which upper and lower layers had the same depth. Then if bathymetry is known, the thermocline depth can be estimated having half of depth in the inversion region. In this paper we explore this possibility by processing some SAR images containing ISWs signatures with polarization inversion in the SE coast of Brazil.

## 2. Data set and Methods

### 2.1 Satellite and auxiliary data set

The SAR images used in this paper are part of a data set consisting in 264 Advanced Synthetic Aperture Radar scenes from September 2009 to December 2010 generated from the ENVISAT/ESA satellite. The satellite data was received and processed by INPE's reception station located in Cachoeira Paulista (22°40'58"S; 45°00'07"W). The images are C-band, VV polarization, Wide-Swath (400x400 km) at a spatial resolution of 150 m with a pixel size of 75m. Most of the images covered the SE Brazilian continental shelf and slope between latitudes of 20° and 28°S, but a fraction of the data set includes deep ocean and a few images south of 28°S (Fig. 1).

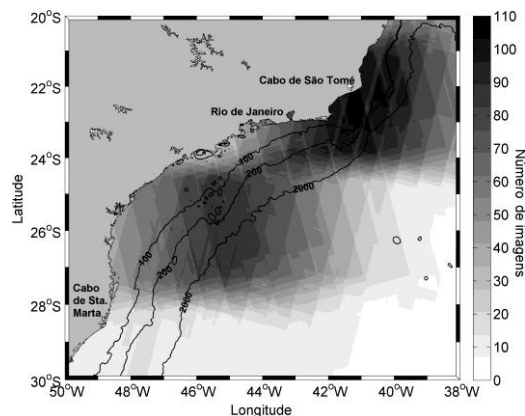


Figure 1. Spatial distribution of ASAR/ESA images received by INPE's station for the period Sep. 2009 to Dec. 2010. Graybar at right: number of scenes per region.

The ISWs are generated from the baroclinic internal tides which are a product of the barotropic tides. To see the characteristics of the tidal signal in the region we used the results of the OTIS (Oregon State University Tidal Inversion Software) model, available at a spatial resolution of  $\frac{1}{4}^\circ$ . The most important tidal component in the region is the M2. For the bathymetry of the region we used ETOPO2 at a spatial resolution of  $2'$  of degree. This depth data set can be downloaded from: <http://dss.ucar.edu/datasets/ds759.3/>. The climatology of density field of the region was calculated from the World Ocean Atlas (WOA09), available at [http://www.nodc.noaa.gov/OC5/WOA09/pr\\_woa09.html](http://www.nodc.noaa.gov/OC5/WOA09/pr_woa09.html) at a spatial resolution of  $1^\circ \times 1^\circ$ . The density field was generated from the salinity and temperature WOA09 data set using the toolbox for Matlab Gibbs-SeaWater (GSW) (McDougall and Barker, 2011).

### 2.2 The theoretical model

Weakly non-linear ISWs are normally modelled using the classical Kortweg de-Vries (KdV) equation:

$$\frac{\partial \eta}{\partial t} + c_0 \frac{\partial \eta}{\partial x} + \alpha_1 \eta \frac{\partial \eta}{\partial x} + \gamma \frac{\partial^3 \eta}{\partial x^3} = 0 \quad (1)$$

where  $\eta$  in our case can be considered the depth of the thermocline,  $c_0$  is linear phase velocity,  $\alpha_1$  is the non-linear coefficient, and  $\gamma$  the dispersion coefficient. The  $\gamma$  coefficient is always positive, corresponding to a negative dispersion of the ISWs given the dispersion relation:  $\omega = c_0 k - \gamma k^3$ , where  $k$  is the wavenumber of the wave (Ostrovsky and Stepanyants, 1989). The non-linear coefficient can be positive or negative depending on the polarization of the wave. For a two-layer ocean, assuming that  $h_1(h_2)$  is the upper (lower) layer depth, we have (Teixeira et al., 2006):

$$A = \frac{1}{3(h_2-h_1)} \left( \frac{2h_1h_2}{\lambda} \right)^2; c_0 = \sqrt{g \left( \frac{\rho_2 - \rho_1}{\rho_2} \right) \frac{h_1h_2}{h_1+h_2}}; \alpha_1 = \frac{3c_0}{2} \left( \frac{h_1-h_2}{h_1h_2} \right); \gamma = \frac{c_0h_1h_2}{6}, \quad (2)$$

where  $\rho_1$  and  $\rho_2$  are the upper and lower layer densities, respectively, and  $g$  is the gravity. The product  $g(\rho_2 - \rho_1)/\rho_2$  is called of reduced gravity and is represented by  $g'$ . The analytical solution for a solitary wave corresponds to the profile of a quadratic hyperbolic secant:

$$\eta(x, t) = A \operatorname{sech}^2 \left[ \frac{x-Ct}{\lambda} \right], \quad (3)$$

where  $A$  is the wave amplitude of the first oscillation,  $C$  is the non-linear phase velocity of the soliton, and  $\lambda$  is the characteristic soliton wavelength (also called “soliton half width”). The non-linear phase velocity  $C$  can be estimated as a function of the linear velocity  $c_0$ :

$$C = c_0 + \frac{A\alpha_1}{3}, \quad (4)$$

Therefore, the velocity of the soliton is proportional to soliton amplitude; the higher the amplitude the faster is its propagation. It is possible to show that when  $h_1 < h_2$ ,  $\alpha_1 < 0$  and  $A$  is negative, i.e. we have a depression wave. If  $h_1 > h_2$ ,  $\alpha_1 > 0$  and  $A$  is positive and we have an elevation wave.

### 2.3 The methodological approach

The procedure used was first to search in the SAR data set for elevation mode type of solitons, i.e. solitons of the type dark/bright  $\sigma_0$  anomalies, measuring from the first soliton of the packet. To each of these elevation solitons we searched the corresponding depression solitons in deeper waters and the position where they started to weaken before the polarization inversion. From the ETOPO2 data set, we extracted the total depth at the region estimated being the inversion region. Half of this depth was assumed as the depth of thermocline ( $h_1$ ) in a simplified two-layer ocean model (Liu et al. 1998).

To estimate the wave amplitude (Eq. 2), besides  $h_1$  and  $h_2$ , we need  $\lambda$ . According to Small et al. (1999),  $\lambda = D/1.32$ , where  $D$  is the distance in the SAR image between the first bright and dark anomalies.

In the sequence, we took some pairs of depression waves in sequence in the SAR images. We assumed that these internal waves were propagating in the same direction, also that the packets were separated by distances close to the wavelength of the internal tide, and were generated in consecutive cycles of the tide in the same region in the shelf break. Considering that these waves were in deep water ( $h_1 \ll h_2$ ), so  $\alpha_1 < 0$  and they could be well represented by KdV equation (Helfrich and Melville, 2006). For each selected wave train first we estimated an average  $C$  by the ratio between sequential wave packets separation and the tidal period ( $M_2$  main component) (Fu and Holt, 1984).

Now, having the average phase speed  $C$ , the upper and lower layer depths ( $h_1$  and  $h_2$ ), and wave amplitude  $A$ , it is possible to estimate the normalized density difference between upper and lower layers,  $\Delta\rho_{norm} = (\rho_2 - \rho_1)/\rho_2$ , which is given by (Teixeira et al. 2006);

$$\Delta\rho_{norm} = C^2 \left\{ g \frac{h_1h_2}{h_1+h_2} \left[ \frac{A(h_2-h_1)}{2h_1h_2} + 1 \right]^2 \right\}^{-1} \quad (5)$$

With the same parameters it is possible to estimate the linear wave speed ( $c_0$ ) and finally the theoretical non-linear  $C$  (Eq. 4) and the non-linear dispersion coefficients  $\alpha_1$  and  $\gamma$  using Eq. 2. The maximum speeds of upper and lower layers  $u_{1max}$  and  $u_{2max}$ , respectively, can be estimated as (Osborne and Burch, 1980):

$$u_{1max} = \frac{c_0 A}{h_1} ; u_{2max} = \frac{c_0 A}{h_2} \quad (6)$$

The limit amplitude of the ISWs ( $A_{lim}$ ), which is the maximum amplitude possible for the solitons was calculated as  $h_2 - H/2$  (Jeans and Sherwin, 2001), where  $H$  is total depth.

Another important quantity is the total energy ( $E_T$ ) per unit of crest length transported by an ISW, which can be calculated from the previous parameter set, and valid for the first soliton of the packet. According to Osborne and Burch (1980) it is given by:

$$E_T = \frac{4}{3}(\rho_2 - \rho_1)gA^2\lambda \quad (7)$$

Where  $(\rho_2 - \rho_1)$  can be estimated multiplying  $\Delta\rho_{norm}$  by an average density of the water ( $1024 \text{ kg m}^{-3}$ ). This expression, although developed for linear waves, have been demonstrated as good approximation for solitary waves (Osborne and Burch, 1980).

### 3. Results and discussion

The published literature about ISWs indicates that elevation mode solitons are a somewhat rare phenomenon (Alpers and Huang, 2011). From a total of 467 packets of ISW observed in all ASAR scenes available, only seven were classified as elevation ISWs, or approximately 1.5% of all occurrences of solitons packets. These cases were observed between  $24^\circ$  and  $28^\circ\text{S}$  and from October to March, i.e. in the spring and summer seasons (See Fig. 2). The elevation ISWs were found between the 45 and 70 m depth waters, at the Medium Continental Shelf (MCS) region (Castro et al. 2006). This is a region characterized by a strong thermocline during the summer. In the winter season, the MCS is very narrow and its stratification is very weak, which makes it difficult to find elevation ISWs in this season.

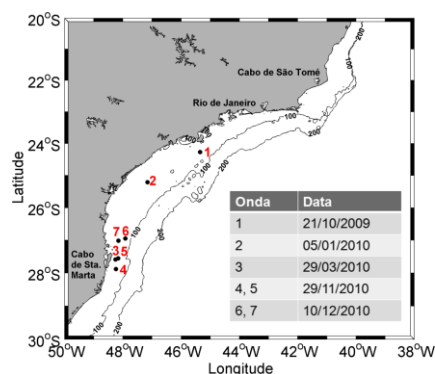


Figure 2. Position and dates for the seven elevation mode ISWs observed from the ASAR data set.

The analysis of the full set of ISWs observed in the region indicate that they are formed as depression waves at shelf break by a non-linear evolution of baroclinic internal tides which propagate predominantly towards the coast (Lorenzzetti and Dias, 2013). Therefore, the presence of the elevation waves at MCS suggests they are formed from an evolution of depression waves in deep water that suffer an inversion of polarization due to the shoaling of the shelf as they move onshore. This inversion of polarization process can be observed in a continuous form in which two packets of ISWs, one of elevation and another of depression are present in the same image (Fig. 3).

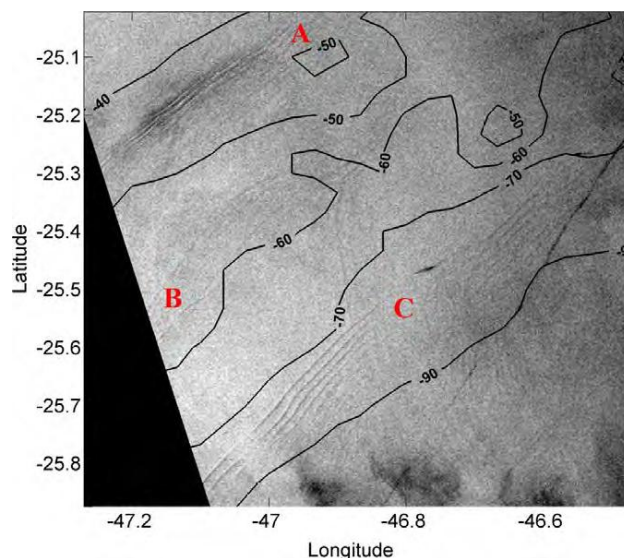


Figure 3. An example of polarization inversion of ISWs. A) Elevation mode; B) Weak transitional phase; and C) Depression mode.

A more detailed view of the  $\sigma_o$  anomalies of the elevation mode ISW observed in the 10 Dec 2010 is given in Fig. 4, where we can see the dark/bright signal characteristic of such mode waves.

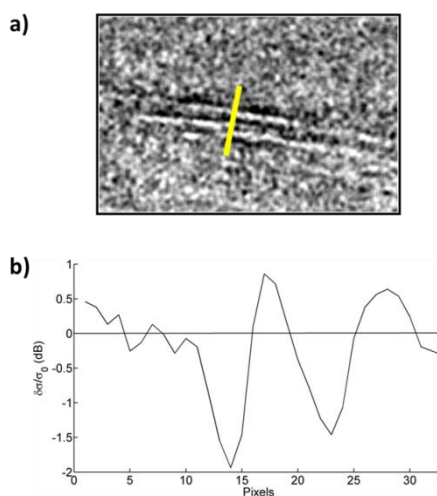


Figure 4. An elevation mode ISW observed day 10 Dec 2010. A) Original SAR image with the yellow line indicating the position of the  $\sigma_o$  transect shown in b) going upper to lower parts of the transect.

Using the ETOPO2 data set and the position of the transition region for each of the cases observed, we estimated from the SAR data the thermocline/pycnocline depth (Table 1). In general, the estimated depth was 30 m, being significantly larger,  $h_1 = 50$  m for the December image. For three cases (05/01, 29/03, and 29/11) there was a better agreement between the estimated and the climatological upper layer thickness. For the 21/10 and 10/12 cases, the estimated  $h_1$  is 100% bigger. We cannot, however, take the climatological data as the “sea truth” since it only represents a long term average; the true unknown  $h_1$  could be, however, near or be sensibly different from it at the time of image acquisition. The presentation of these climatological values was to get some feeling about the order of magnitude comparison against what was the only available in situ data set. What can be said is that the estimated

values are of the same order of magnitude as those expected for the relative months at the region.

Table 1 – Day, position, estimated and climatological depth of thermocline ( $h_1$ ) for the cases of observed elevation ISWs.

Day	Longitude	Latitude	$h_1$ (m)	
			Estimated	Climatology
21/10/2009	45.35° W	24.26° S	30	15
05/01/2010	47.15° W	25.20° S	30	25
29/03/2010	48.25° W	27.58° S	30	25
29/11/2010	48.24° W	27.88° S	30	40
10/12/2010	47.90° W	27.01° S	50	25

The Table 2 presents the estimated values obtained from the depression mode ISWs selected for in the study area using the theoretical formulation presented above.

Table 2 – ISW and water column parameter values as estimated from the solution of the two-layer model KdV equation.

	A) 05 Jan. 2010	B) 29 Mar. 2010	C) 10 Dez. 2010		
<b>C (m/s)</b>	0.7	0.64	0.74	0.82	0.87
<b>H (m)</b>	75	150	90	135	145
<b><math>\lambda</math> (m)</b>	284	379	189	189	227
<b>A (m)</b>	2	1.33	4.51	5.8	12.94
<b><math>A_{lim}</math> (m)</b>	7.5	45	15	37.5	22.5
<b><math>\Delta\rho_{norm}</math> (<math>\times 10^{-3}</math>)</b>	2.7	1.7	2.3	2.4	2.1
<b><math>c_0</math> (m/s)</b>	0.69	0.63	0.71	0.77	0.82
<b><math>u_{1max}</math> (cm/s)</b>	4.63	2.8	10.62	14.8	21.33
<b><math>u_{2max}</math> (cm/s)</b>	-3.08	-0.7	-3.54	-3.29	-11.23
<b><math>\alpha_1</math> (<math>\times 10^{-2}</math>)</b>	-1.1	-2.3	-2.3	-2.9	-1.1
<b><math>\gamma</math></b>	155.76	377.45	317.52	516.38	652.31
<b>Crest length (km)</b>	45	44	85	52	61
<b><math>E_T</math> (J)</b>	$1.8 \times 10^9$	$5.2 \times 10^8$	$10^{10}$	$10^{10}$	$6.7 \times 10^{10}$

The estimated characteristic wavelengths ( $\lambda$ ) were larger than those reported for the ISWs observed at Portuguese continental shelf ( $\lambda_{max}=180m$ ), but smaller than for the China Sea ( $\lambda_{max}=1km$ ) (Zheng et al., 2001). We should say, however, that with a pixel size of 75m and a  $\lambda$  ranging from 189 to 379 m, we could have an error of about 20 – 40%. The image resolution also might be affecting the estimate of the ISWs amplitude since an error in the estimation of  $\lambda$  goes quadratically into A (See Eq. 2). ISW amplitude ranged between 1.3 and 13 m, which compared to their limit values ( $A_{lim}$ ) indicate they were of small to medium amplitude. Similar ISW amplitudes estimated from SAR imagery have been reported by Zheng et al. (2001) and Teixeira et al. (2006), but these are small amplitudes when compared to strong ISW cases for which the amplitudes can reach about 90 m (Apel et al., 1985). The lack of in situ observations for our region precludes any definitive conclusion about the possible presence of such intense large-amplitude ISW there. The largest thermocline depth ( $h_1=50m$ ) estimated for the 10 Dec 2010 image is associated with the largest amplitude ISW ( $A \approx 50m$ ) and highest surface layer currents ( $u_1 \approx 21$  cm/s). The non-linear coefficients ( $\alpha_1$ ) were in general smaller than those found by Teixeira et al. (2006) for the China Sea, but our dispersion coefficients ( $\gamma$ ) were generally larger. Probably these differences are due to deeper waters for the regions where our ISWs were found. The non-linear phase speeds (C) determined from the two-layer model solutions (Eq. 4) shown in the first line of Table 4, are

very similar to the values reported by Lorenzetti and Dias (2013) determined simply by dividing the separation of ISWs by the M2 tidal period for the same data set (their Fig. 13). Although the initial estimate of  $C$  has entered into the parameter set, it is still interesting to compare the final non-linear soliton theoretical speed, which depends on three parameters,  $A$ ,  $c_0$ , and  $\alpha_1$ , to the statistical values derived from the full data set not using the two-layer model.

It should be noted that the ISWs in the region, although not so intense, can transport large amounts of energy ( $E_T$ ). The highest value found for our data set was  $6.7 \times 10^{10}$  J per unit length, leading to approximately 4.1 MJ for the 61 km of crest length. Dividing this value by the time it takes for the solitons to pass, which is nearly  $\lambda/C$ , or 261 s ( $\sim 4$  min), we would get about 16 MW/km of wave crest.

A crude check on the estimated and climatological density contrast between upper and lower layer densities is presented in Fig. 5 for the months of January, March, and December and for the coordinates close to those shown in Table 1. For Jan and Mar we used the average values of  $\Delta\rho_{\text{norm}}$ , and for Dec the only value available. These normalized density differences were multiplied by  $1024 \text{ kg m}^{-3}$  taken as a mean water density. A two-layer representation of the stratification using the average  $h_1$  depth and  $\Delta\rho_{\text{norm}}$  are presented in Fig. 5. The two-layer results obtained, although a crude representation for the continuum vertical density stratification, agree reasonably well to it.

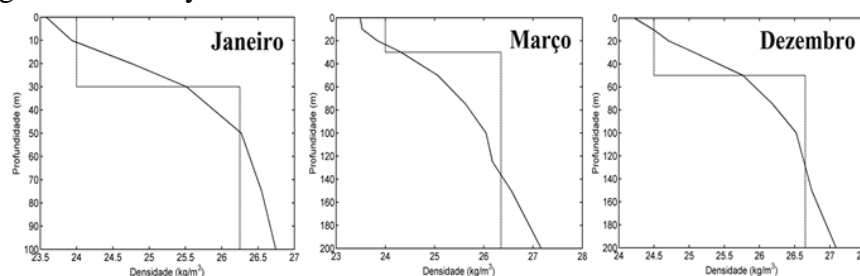


Figure 5. Two-layer representation estimated from SAR image analysis against climatological density profiles (WOA09 data set). From left to right: January, March, and December.

#### 4. Conclusions

We described in this paper the procedure that can be used to extract from an analysis of pattern of ISWs that show a polarization inversion a series of parameters describing the characteristics of such solitons (linear, non-linear wave speed, amplitude, non-linear coefficient, dispersion coefficient), and of the water column, such as depth of thermocline and density contrast between upper and lower layers. The analysis of the full data set showed that elevation mode ISWs are, however, a very rare event in the region (nearly 1.5% of cases), and that they probably occur mostly during the spring and summer seasons. The  $h_1$ ,  $h_2$ , and density contrast between upper and lower layer seems coherent to the climatological monthly stratification as given by the WOA09 data set. The results indicate that the ISWs observed are of the small to medium size as compared to maximum possible and to other high energy regions of the world ocean. Maximum upper layer velocities estimated for these solitons was on the order of  $20 \text{ cm s}^{-1}$ . We think that with the availability of a higher resolution set of SAR images of the region it will be possible to better estimate the theoretical parameter set and refine the results here presented. The high energy of these waves is ultimately being dissipated into turbulence in the shallower depths of the shelf. It is, therefore, reasonable to expect that the ISW breaking turbulence might have some influence in the physical and ecosystem properties this shelf.

#### References

Apel, J.R.; Gonzalez, F.I. Nonlinear features of internal waves off Baja California as observed from the Seasat imaging radar. **Journal of Geophysical Research**, v. 88, n. 7, p. 4459– 4466, 1983.

Apel, J.R.; Holbrook, J.R.; Liu, A.K.; Tsai, J.J. The Sulu Sea internal solitons experiment. **Journal of Physical Oceanography**, v. 15, p. 1625-1651, 1985.

Alpers, W.; Huang, W. On the discrimination of radar signatures of atmospheric gravity waves and oceanic internal waves on synthetic aperture radar images of the sea surface. **IEEE Transactions on Geosciences and Remote Sensing**, v. 49, n. 3, p. 1114-1126, 2011.

Castro, B.M.; Lorenzetti, J.A.; Silveira, I.C.A.; Miranda, L.B. Estrutura termohalina e circulação na região entre o cabo de São Tomé (RJ) e o Chuí (RS). In: Rossi-Wongtschowski, C.L.D.B.; Madureira, L.S-P. (Org.). **O ambiente oceanográfico da plataforma continental e do talude na região sudeste-sul do Brasil**. São Paulo, SP: Edusp, 2006. cap. 1, p. 11-120.

da Silva, J.C.B.; New, A.L.; Azevedo, A. On the role of SAR for observing local generation of internal solitary waves off the Iberian Peninsula. **Canadian Journal of Remote Sensing**, v. 33, n. 5, p. 388–403, 2007.

Fu, L-L.; Holt, B. Internal waves in the Gulf of California: observations from a spaceborne radar. **Journal of Geophysical Research**, v. 89, n. C2, p. 2053– 2060, 1984.

Helfrich, K.R.; Melville, W.K. Long nonlinear internal waves. **Annual Review of Fluid Mechanics**, v. 38, p. 395-425, 2006.

Jeans, D.R.G.; Sherwin, T.J. The variability of strongly non-linear solitary waves observed during an upwelling season on the Portuguese shelf. **Continental Shelf Research**, v. 21, p. 1855-1878.

Liu, A.K.; Chang, Y.S.; Hsu, M-K.; Liang, N.K. Evolution of nonlinear internal waves in the East and South China Seas. **Journal of Geophysical Research**, v. 103, n. C4, p. 7995– 8008, 1998.

Lorenzetti, J.A.; Dias, F.G. Internal Solitary Waves in the Brazilian SE continental shelf: Observation by Synthetic Aperture Radar. **International Journal of Oceanography**, v. 2013, 11pp., Article ID 403259, dx.doi.org/10.1155/2013/403259.

McDougall, T.J.; Barker, P.M. Getting started with TEOS-10 and the Gibbs Seawater (GSW) Oceanographic Toolbox. SCOR/IAPSO WG1227, ISBN 978-0-646-55621-5, 28pp., 2011.

Osborne, A.R.; Burch, T.L. Internal solitons in the Andaman Sea. **Science**, v. 208, n. 4443, p. 451-460, 1980.

Ostrovsky, L.A.; Stepanyants, Y. Do internal solitons exist in the ocean? **Rev. Geophys.**, v. 27, n. 3, p. 293-310, 1989.

Small, J.; Hallock, Z.; Pavey, G.; Scott, J. Observations of large amplitude internal waves at the Malin Shelf edge during SESAME 1995. **Continental Shelf Research**, v. 19, n. 11, p. 1389-1436.

Teixeira, M.; Warn-Varnas, A.; Apel, J.; Hawkins, J. Analytical and observational studies of internal solitary waves in the Yellow Sea. **Journal of Coastal Research**, v. 22, n. 6, p. 1403-1416, 2006.

Zheng, Q.; Yuan, Y.; Klemas, V.; Yan, X-H. Theoretical expression for an ocean internal solitons synthetic aperture radar image and determination of the solitons characteristic half width. **Journal of Geophysical Research**, v. 106, n. C11, p. 31415– 31423, 2001.